ADVANCEMENTS IN 3D CONCRETE PRINTING WITH GEOPOLYMER BINDERS

Sahil Kaushik*

Abstract

The construction industry is experiencing a transformative shift propelled by Additive Manufacturing (AM), commonly known as 3D printing. Despite widespread adoption in various sectors, the construction industry has been cautiously exploring AM's potential. This paper investigates the transformative power of AM, particularly in 3D Concrete Printing (3D-CP) using geopolymer binders.

Historically, construction relied on conventional methods like pouring concrete into formworks. However, AM offers compelling advantages, including unparalleled design freedom, heightened safety, cost efficiency, waste reduction, and accelerated project timelines. Within the domain of 3D-CP, our focus is on powder-based techniques, involving precise deposition of powdered materials to craft intricate architectural forms. The synergy of these technologies with concrete opens doors to innovative construction possibilities.

Our research delves into powder-based 3D Concrete Printing (PB-3D-CP), with a specific emphasis on geopolymer-based powders. Through a thorough exploration of experimental methodologies, we investigate particle size distributions, bed surface quality, densities, wettability, and mechanical properties. Our objective is to unearth insights that not only advance our understanding of this technology but also contribute to the broader discussion on the convergence of AM and construction.

Keywords: Additive Manufacturing (AM), 3D Printing, Concrete Printing, Geo-Polymer

*Om Sterling Global University Hisar, IEI – Civil, Associate Member sahilkaushik.8302@gmail.com

***Corresponding Author:** Sahil Kaushik
*Om Sterling Global University Hisar, IEI – Civil, Associate Member sahilkaushik.8302@gmail.com

DOI: 10.17628/ecb.2020.9.33-38

Introduction

In recent times, the construction industry has undergone a profound transformation, powered by the rapid advancements in Additive Manufacturing (AM), more commonly known as 3D printing. AM introduces an innovative manufacturing approach wherein intricate 3D structures, meticulously designed using computer-aided software, materialize through a layer-by-layer deposition process, crafting complex objects from a series of cross-sectional slices [1,2]. While industries like automotive, aerospace, medicine, and biotechnology have fully embraced the potential of AM [1,3], the construction sector has cautiously navigated this game-changing technology.

Traditionally, construction relied on conventional methodologies, often involving the pouring of concrete into formworks to bring architectural visions to life. However, recent years have witnessed a gradual shift as the construction industry increasingly turns its attention to the possibilities offered by AM. The allure of this technology lies in its manifold advantages over traditional methods. Primarily, it offers unprecedented geometric freedom, enabling the realization of architectural forms and structures previously unimaginable. Furthermore, the integration of additive manufacturing into the construction industry promises enhanced safety, reduced construction costs, minimized waste generation, and shorter project timelines [4,5]. The amalgamation of these factors serves as a compelling invitation for the construction industry to explore the potential of AM in redefining how structures are conceptualized and constructed.

At the heart of this transformative wave lies the domain of 3D concrete printing (3D-CP), representing a fascinating fusion of technology and construction. In recent years, a plethora of AM technologies has been meticulously developed to find relevance in 3D-CP applications. Notably, these technologies manifest in two distinct forms: extrusion-based and powder-based techniques. The former entails precise concrete extrusion to construct structures layer by layer, while the latter presents a unique paradigm where powdered materials are thoughtfully deposited to craft intricate architectural forms. The synergy between these technologies and concrete opens doors to innovative construction possibilities, setting the stage for a future where buildings may emerge in unprecedented shapes and sizes.

This paper embarks on a journey into the confluence of AM and the construction sector, with a specific focus on the advancements made in powder-based 3D Concrete Printing (PB-3D-CP) techniques. Through intricate exploration of experimental methodologies, this study seeks to uncover the potential of geopolymer-based powders in the realm of 3D-CP. By scrutinizing particle size distributions, bed surface quality, densities, wettability, and mechanical properties, this research aims to unearth insights that not only advance our understanding of this technology but also contribute to the broader discourse on the intersection of AM and construction.

As we delve into the intricate fabric of PB-3D-CP and its promise within the construction domain, it becomes increasingly evident that we stand at the cusp of an era where innovation and technology reshape the very contours of architectural creation. The subsequent sections of this paper undertake a meticulous journey, unveiling the nuances of experimental procedures, discussing results, and culminating in meaningful conclusions that underscore the significance of PB-3D-CP in redefining the built environment.

2. 3-D Printing Techniques

2.1 3D Concrete Printing through Extrusion

The extrusion-based methodology constitutes an innovative additive manufacturing (AM) process, wherein concrete is systematically extruded through a specialized nozzle. This nozzle is often affixed to a gantry, crane, or robotic arm, enabling precise layer-by-layer deposition. Noteworthy exemplars of this technique include Contour Crafting, an endeavor pioneered by Khoshnevis [6,7], and concrete printing, a brainchild of Lim et al. [8,9]. The extrusion-based approach in 3D concrete printing (3D-CP) is strategically tailored for on-site construction endeavours, particularly for crafting large-scale architectural elements characterized by intricate geometries.

2.2 3D Concrete Printing Utilizing Powder-Based Technology

The paradigm of 3D Concrete Printing using powder (3D-CP) stands as another hallmark of additive manufacturing (AM), delivering meticulous structures characterized by intricate geometries. In this method, precise structures are fashioned through the selective deposition of binder liquid, akin to "ink," onto a powder bed. The resultant binding of the powder where it interacts with the bed is foundational to this process [10]. Cesaretti et al. [11] illustrates the instances of this technique include the D-shape method and the innovative Emerging Objects concept spearheaded by Rael et al. [12]. Notably, the 3D concrete printing using powder methodology finds its forte in offsite manufacturing of precast components, primarily tailored for the creation of small-scale building elements such as panels, permanent

formworks, and interior structures. Subsequently, these components can be assembled at the construction site.

This paper's focal point resides in the realm of powder-based 3D-CP, chosen due to its ability to fabricate building components that embody intricate details and elaborate forms. The construction industry's appetite for such components, which conventionally entail costly formwork systems, drives the demand for an alternative. The powder-based 3D-CP approach, with its potential to produce durable components at an expedited pace, answers this demand and underscores the urgency for dedicated research in this sphere.

Figure 2.1 illustrates the powder-based 3D-CP process. It commences with a roller and a print head applying a 3 mm thick foundational layer of powder to the build plate. Then, a 0.1 mm thin layer is evenly distributed and smoothed by the roller, determined by the 3D printer's layer thickness setting. After each layer, the print head dispenses binder solution through nozzles using a drop-on-demand technique, either thermally or mechanically. This precise delivery forms binder droplets, adhering powder particles. Iteratively, the final part takes shape, later removed after drying, with excess unbound powder expelled by an air blower.

The potential of the 3D Concrete Printing using powder technique to revolutionize the construction industry is profound, yet several obstacles necessitate overcoming before its full utilization becomes a reality. Chief among these challenges is the limitation posed by proprietary printing materials commonly utilized in commercially available powder-based 3D printers, rendering them unsuitable for construction applications. Consequently, there is a pressing urgency to broaden the horizons of materials compatible with 3D printing utilizing powder, transcending the current constrained scope.

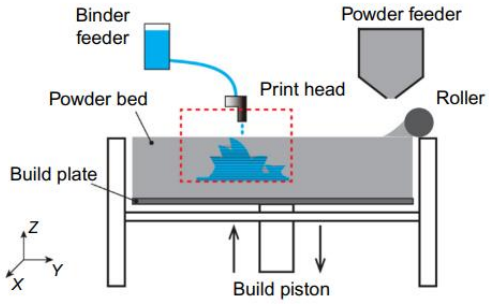

Figure 2.1 Schematic illustrations of the 3D printing process

Geopolymer, an inorganic binding agent in concrete, offers a promising alternative [13,14]. These alkali aluminosilicate cements often outperform Ordinary Portland Cement, with reduced CO2 emissions. Geopolymers are synthesized using aluminosilicate precursors and alkaline activators, showcasing impressive properties like compressive strength, resistance to sulfate, acid, and minimal creep. Using industrial byproducts like slag and fly ash is appealing due to waste disposal concerns. Exploring novel methods like powder-based 3D-CP holds potential to expand geopolymer applications.

Fly ash-based geopolymers offer advantages over slag-based ones, including enhanced fire resistance and reduced shrinkage and creep [15]. Fly ash is abundant but often underutilized, while slag sees higher usage in concrete production. The challenge lies in fly ash geopolymers requiring high-temperature curing (around 60°C), unlike slag-based ones that set at room temperature. This constraint impacts the applicability of fly ash in powder-based 3D-CP, necessitating a minimum inclusion of slag for setting at ambient conditions.

3. EXPERIMENTAL PROCEDURES

3.1 Materials - Powder

Low calcium (Class F) fly ash and granulated ground blast furnace slag (slag) were sourced from the local suppliers. The chemical composition of the fly ash and slag, as analyzed through X-ray Fluorescence, is tabulated in Table 3.1. The percentages in total do not sum to 100% due to rounding.

Anhydrous sodium metasilicate powder, available as beads was employed as the alkaline activator for this research. Its chemical composition includes 50.66 wt% Na_2O, 47.00 wt% SiO_2, and 2.34 wt% H_2O. Additionally, a high purity silica sand, with a median size of 184 µm was incorporated. The post-processing of green samples involved the use of sodium hydroxide solution and N Grade sodium silicate. The N Grade sodium silicate solution, exhibited a modulus (Ms) of 3.22, where Ms = SiO_2/Na_2O (with Na_2O at 8.9 wt% and SiO_2 at 28.6 wt%). In the case of the NaOH solution, a concentration of 8.0 M was prepared by utilizing 97% pure NaOH beads from Sigma-Aldrich along with tap water.

This study encompassed the investigation of five distinct geopolymer powders, each characterized by varying slag to fly ash ratios, as depicted in Table 3.2. To compose each mixture, the alkaline activator (beads) was initially subjected to a 5-minute grinding process using a planetary ball mill, maintaining a powder-to-ball mass ratio of 0.3. Following this, a comprehensive dry mixing procedure was carried out in a Hobart mixer, combining fly ash, slag, silica sand, and the ground activator powder. The resultant mixture achieved a uniform state of homogeneity, confirmed through visual observation.

Chemical	Component	
	Slag	Fly ash
Al_2O_3	12.37	25.56
SiO_2	32.76	51.11
CaO	44.64	4.30
Fe_2O_3	0.54	12.48
K_2O	0.33	0.70
MgO	5.15	1.45
Na_2O	0.22	0.77
P_2O_5	0.88	0.01
TiO_2	0.51	1.32
MnO	0.15	0.37
SO_3	4.26	0.24
LOI[a]	0.09	0.57

[a]Loss on ignition.

Table 3.1 The chemical composition of slag and fly ash (weight%)

A schematic outlining the procedure for preparing geopolymer powder is depicted in Fig. 3.2.

Mix ID	Geopolymer precursors wt%	
	Slag	Fly ash
S100FA0	100	0
S75FA25	75	25
S50FA50	50	50
S25FA75	25	75
S0FA100	0	100

Table 3.2 Mix Proportions of geopolymer precursors

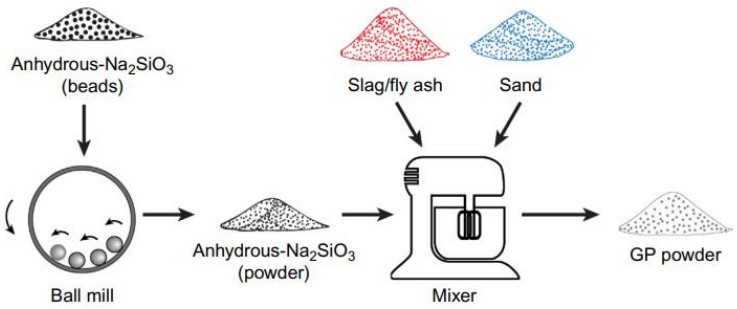

Figure 3.1 The process of preparing geopolymer powder

3.1.1 Binder

The 3D-CP procedure employed an aqueous solvent (Zb 63) as a binder. The commercial clear aqueous Zb 63 binder has a viscosity that is comparable to that of pure water. According to an examination of Zb 63 with the help of Fourier transform infrared spectroscopy [16], it was primarily composed of water and 2-Pyrrolidone.

3.2 Print-ability of Geopolymer Powder

According to Butscher et al. (17), The essential prerequisites for the 3D Concrete Printing (3D-CP) process are the ability to print and deposit powder. The printability factor is impacted by various characteristics of the powder, including particle size distribution, true/bulk densities, porosity of the powder bed, and the behaviour of binder droplet penetration. Prior to integrating a new powder into a commercially accessible 3D printer, it's imperative to evaluate its printability [17].

3.2.1 Particle Size Distribution

The laser diffraction particle analyzer (Cilas 1190, CILAS, France) was employed to assess the

particle size and particle size distribution (PSD) of the powders. Each powder underwent three measurements to determine the D10, D50, and D90 values, representing the sizes below which 10%, 50%, and 90% of the particles fall, respectively.

3.2.2 Powder Bed Surface Quality

Upon completing the arrangement of the powder bed within the printer, the build plate containing the powder bed was taken out from the 3D printer. A Nikon D810 camera was employed to examine the surface qualities of both powder beds. The inspection was carried out at a 45-degree angle relative to the top of the powder bed.

3.3 True, Bulk, and In-Process Powder Bed Densities

The true ($\rho_{true.powder}$) and bulk ($\rho_{bulk.powder}$) densities of the powders were determined following the guidelines of International Standard AS-1774.6-2001 (R2013) for true density measurement and AS-1774.2-2001 (R2013) for bulk density measurement. In-process bed density ($\rho_{bed\ powder}$), initially proposed by Zhou et al. [18], refers to the density assessed after the powder is evenly distributed on the build plate. This parameter is crucial to ensuring high printing quality in the 3D Concrete Printing using powder (3D-CP) process.

To measure in-process bed density, the powder was first spread onto the build plate using a roller from the powder feeder. Subsequently, the build plate was extracted from the 3D printer. The mass of powder on the build plate and the volume of the powder bed were both measured to determine the in-process bed density. Powder bed porosity (P_{bed}) can be calculated using the equation below.

$$P_{\text{bed}} = 1 - \frac{\rho_{\text{bed.powder}}}{\rho_{\text{true.powder}}} \times 100\%$$

3.4Drop Penetration Behaviour and Wettability

The build plate was removed from the 3D printer when the powder bed was fully prepared over it. Subsequently, a binder droplet (Zb 63) with an approximate volume of 60 µL was deposited onto the powder bed surface with the help of 1 mL medical syringe fitted with a 25-gauge needle. The droplet began to form at the needle's tip and expanded until its weight surpassed the force of surface tension.

In this investigation, the powder's wettability was assessed through three parameters (Fig. 11.3B): drop penetration time (t_p), drop penetrating depth (d_p), and the drop spreading diameter (ϕ_p). Drop penetration time (t_p) signifies the time taken by the droplet to fully infiltrate the powder, leaving behind no liquid onto the surface of powder bed. The progress made by single binder droplet to infiltrate the powder bed was monitored by a high-speed video recorder operating at 240 frames/second. Ten trials were carried out for each powder, and the drop penetration time was deduced from the video frame by frame. The beginning of the process was designated as the moment the binder droplet first made contact with the powder bed, while the conclusion was determined by the point when the light reflection on the droplet ceased.

Spreading diameter (ϕ_p) and drop penetrating depth (d_p) were determined with the help of a digital calliper with a precision of 0.01 mm once the granule solidified. An air blower and a sieve were utilized to eliminate the unbound powder. These two measures were taken subsequent to each drop penetration time evaluation. For each blend of powder, measurements of t_p, d_p, and ϕ_p were conducted ten times.

3.5 3D Concrete Printing Utilizing Powder – Process

A Solid Works-designed cube model of size 20 mm served as the blueprint for printing. The study utilized the 3D concrete printing utilizing powder process, conducted on a commercially available 3D printer, the Z-printer 150 from Z-Corp. The printing was facilitated through an HP11 print head (C4810A). The 3D printer is equipped with a specified resolution of 300 x 450 dots / inch (dpi) and boasts a build volume of 185 x 236 x 132 mm. For the sake of simplicity, the default parameters for printing were employed. These included a layer of thickness 0.102 mm and ratio of binder-to-volume as 0.24 for the shell section and 0.12 for the core section of the printed structure. Following a 6-hour drying period within the powder bed, the removal of unbound powder was executed through a de-powdering process utilizing compressed air.

3.6 Postprocessing Procedure

After de-powdering step, the printed cubes were segregated into two distinct groups. The first group, labelled as "green samples," underwent no further postprocessing steps. The second group, referred to as "postprocessed samples," experienced additional treatment. These printed cubes were submerged in an alkaline solution and then subjected to an oven set at a temperature of 60 ± 3°C for a duration of 7 days. The alkaline solution used was a blend of N Grade sodium silicate solution characterized by a SiO_2/Na_2O ratio of 3.22 (comprising 71.4% w/w) and an 8.0 M NaOH solution (constituting 28.6% w/w). Upon the culmination of the heat-curing duration, the postprocessed samples were taken out from the oven and allowed to cool without any disturbances.

3.7 Mechanical Properties - Compressive Strength

The compressive strength of the green and postprocessed samples in both the X-direction and Z-direction were measured under load control at the rate of 0.33 MPa/s. A population of 10 samples for each testing direction was used.

4 RESULTS AND DISCUSSIONS

4.1 Powder Characteristics

Figure 4.1 illustrates the particle size and particle size distribution characteristics of geopolymer powders. These geopolymer powders, encompassing various ratios of slag to fly ash, exhibit particle sizes spanning the range of 0.1 to 100 µm. Notably, the initial fly ash and slag in their raw forms used for powder production possess D50 values of 3.74 µm and 12.68 µm, respectively. Consequently, the incorporation of fly ash into the geopolymer powder formulation leads to a leftward shift in the cumulative frequency curve.

In the 3D Concrete Printing utilizing powder (3D-CP), the particle size and PSD hold critical importance for achieving optimal powder deposit ability, thereby ensuring the creation of a uniform and seamless powder bed [19,20]. This factor significantly influences the surface quality of both ZP and GP materials during the printing process. Observations indicated that all the geopolymer powders displayed satisfactory surface qualities suitable for the 3D Concrete Printing utilizing powder (3D-CP).

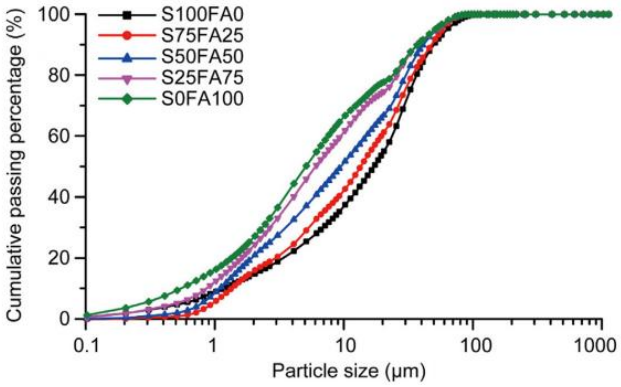

Fig 4.1 Particle size distributions of geopolymer powders

4.2 True/Bulk Densities, In-Process Bed Density, and Powder Bed Porosity

Table 4.1 provides a summary of the true/bulk densities, in-process bed density, and powder bed porosity for each geopolymer powder.

The incorporation of higher quantities of fly ash in the geopolymer powder formulation resulted in a decrease in the true, bulk, and in-process bed densities of the powder. Conversely, this increase in fly ash content led to a rise in powder bed porosity. However this impact was not particularly substantial. Across the various geopolymer powder blends, the minimal difference observed between bulk density and in process bed density suggests that the powder underwent limited compression during the spreading process.

Powder properties	Mix ID				
	S100FA0	S75FA25	S50FA50	S25FA75	S0FA100
True density (g/cm^3)	2.81	2.73	2.66	2.59	2.51
Bulk density (g/cm^3)	0.78	0.76	0.75	0.72	0.69
In-process bed density (g/cm^3)	0.83	0.81	0.78	0.75	0.73
Powder bed porosity (%)	70.4	70.4	70.6	71.0	70.9

Table 4.1 True/bulk densities, in-process bed density, and powder bed porosity of geopolymer powder

4.3 Binder Droplet Penetration Behaviour

In Fig. 4.2, visual representations showcase the characteristic behaviour of binder droplet penetration in the geopolymer powders.

With an increase in fly ash content within the geopolymer powder, the required time for complete penetration of the binder droplet into the powder bed also increased. This implies that properties of the powder, including powder density as well as particle size and shape, play a role in influencing the behaviour of binder droplet penetration.

Upon successful binder droplet penetration, solid granules formed within the powder bed. These granules possessed sufficient green strength, allowing for the measurement of dp and ϕp, except in the case of the S0FA100 mix, which contained 100% fly ash. For this particular geopolymer powder with 100% fly ash, the limited reactivity led to granules too weak to endure the pressure during the de-powdering process.

As indicated in Table 4.2, the geopolymer powder consisting of 100% slag (S100FA0) exhibited the shortest binder droplet penetration time. Conversely, the longest tp was noted for the S0FA100 powder with 100% fly ash, clocking in at 73% longer than that of the S100FA0 powder. Greater fly ash content in the geopolymer powder corresponded to finer average particle size, leading to prolonged binder droplet penetration time. According to Hapgood [21], alterations in particle size affect the pore structure within the powder bed. Fine particles tends to aggregate, resulting in numerous macro-voids in the bed. Consequently, the binder liquid travels through micro-voids around these macro-voids, significantly extending the penetration time. Thus, geopolymer powders with higher fly ash content featuring finer particle sizes tend to exhibit longer binder droplet penetration times.

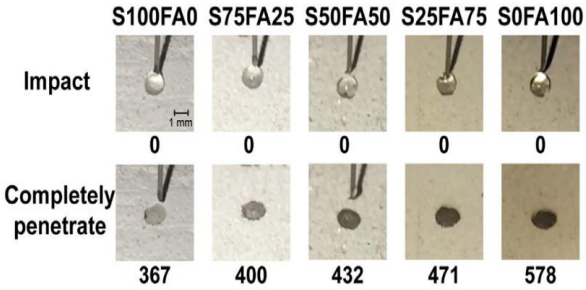

Figure 4.2 Binder droplet images created on surface of geopolymer powder beds. Number written below the image shows the droplet penetration time (ms)

Mix ID	Binder droplet penetration parameters		
	t_p[a] (ms)	d_p[b] (mm)	φ_p[c] (mm)
S100FA0	335 ± 42	2.10 ± 0.21	1.95 ± 0.16
S75FA25	370 ± 64	2.46 ± 0.22	1.82 ± 0.11
S50FA50	440 ± 57	2.78 ± 0.29	1.72 ± 0.15
S25FA75	490 ± 43	2.90 ± 0.18	1.67 ± 0.16
S0FA100	580 ± 76	–[d]	–[d]

[a]Binder droplet penetration time.
[b]Binder droplet penetration depth.
[c]Binder droplet spreading diameter.
[d]Could not be measured due to weak strength of granules made with this powder.

Table 4.2 Binder droplet penetration behaviour results of geopolymer podwer

Table 4.2 provides a summary of tp, dp, and ϕp values for each geopolymer powder. The values presented in the table are averages based on 20 measurements, with reported errors reflecting a 95% confidence level.

Conversely, an augmentation in fly ash content within the geopolymer powder led to a reduction in ϕ_p. According to Nefzaoui et al. [22], ϕ_p hinges on the physicochemical attributes of the binder droplet and the hydrophilicity of the powder bed surface. Thus, the diminished ϕ_p observed in geopolymer powders with elevated fly ash content could be attributed to the decrease in hydrophilicity of the powder bed surface, stemming from the decrease in average particle size of geopolymer powder.

On the contrary, the geopolymer powder comprising 100% slag (S100FA0) registered the shallowest binder droplet penetration depth (d_p). As the fly ash content increased, so did the d_p of the geopolymer powder. In general, binder droplet penetration follows the spreading phase. For a constant-volume binder droplet, a smaller spreading diameter implies a greater penetration depth—requiring the droplet to delve deeper into the powder bed for complete penetration. Hence, it is logical to conclude that the S100FA0 powder displayed the smallest dp while simultaneously showcasing the largest ϕp.

4.4 Mechanical Properties

In Fig. 4.3, visual representations showcase the 3D printed cubes generated using geopolymer powders of varying slag-to-fly ash ratios. However, no sample could be printed from the geopolymer powder comprising 100% fly ash (S0FA100). The inability to print from this powder was attributed to its low reactivity with the binder liquid under ambient conditions. Consequently, there is no available data for the S0FA100 powder in relation to linear dimensional accuracy and compressive strength outcomes.

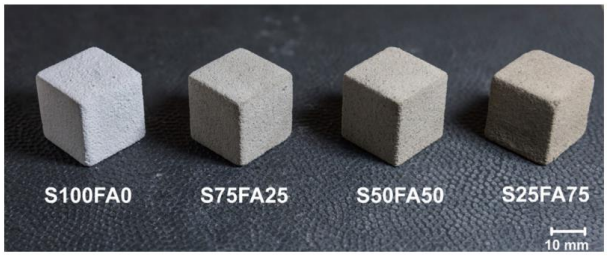

Figure 4.3 3D printed green cubes using geopolymer powder with different slag/fly ash ratio

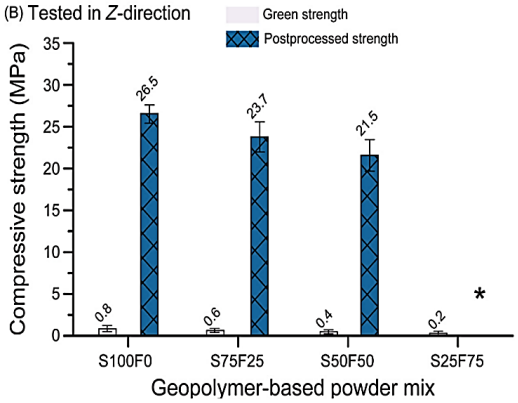

The 3D printed cubes' uniaxial compressive strengths over a span of 7 days, both for the green and postprocessed variations, are depicted in Fig. 4.4. It's crucial to emphasize that the S25F75 samples underwent dissolution in the curing solution during the postprocessing stage. Consequently, no data is available concerning the compressive strength of the postprocessed S25FA75 samples.

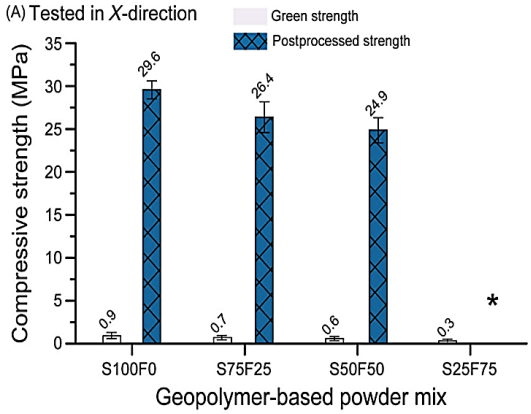

Fig. 4.4. The 7-day uniaxial compressive strength of green and postprocessed 3D cubes measured in (A) the X-direction and (B) the 2-direction.

4.4.1 Green Samples

As depicted in Figure 4.4, the green samples displayed relatively moderate levels of compressive strength, increasing from 0.24 and getting upto 0.91 megapascals (MPa), contingent upon the direction of testing and the fly ash content. It's crucial to highlight that this degree of strength suffices for the de-powdering process.

In both testing directions, an increase in fly ash content corresponded to a significant decrease in the compressive strength of the green samples. This

decline is attributed to the subdued reactivity of fly ash under ambient temperatures.

A pronounced anisotropic behaviour was also observed in the compressive strength of the green samples, contingent upon the directions of loading. Irrespective of the fly ash content, the compressive strength consistently exceeded the strength in the Z-direction when assessed in the X-direction. To be precise, the green compressive strength of S100FA0, S75FA25, S50FA50, and S25FA75 samples in the X-direction was respectively 20%, 25%, 41%, and 42% higher compared to their corresponding strengths in the Z-direction.

This anisotropic phenomenon is likely linked to the preferential orientation of powder particles during the spreading process [23]. Within the layers of powder, larger facets of particles tend to align parallel to the X-Y plane, and the smaller facets with sharper edges become more prominent in the Z-direction. The gel formed between these larger facets is more robust compared to the gel formed between the smaller facets. Consequently, greater energy is required to rupture the bonds between these larger facets of powder particles.

4.4.2 Postprocessed Samples

As illustrated in Fig. 4.4, the postprocessed samples displayed considerably higher compressive strength compared to the green samples in both testing directions. This holds true regardless of the fly ash content. The postprocessed compressive strength after 7 days ranged from 21.5 to 29.6 megapascals (MPa), contingent upon fly ash content and testing direction. This range fulfils the compressive strength requirements for numerous applications within the construction industry.

In X-direction, the samples exhibit 32, 37 and 41 times more compressive strength than that of corresponding green samples. Similarly in Z-direction, the compressive strength of post-processed sample was 33 to 54 times higher than that of the corresponding green samples. This boost in strength is attributed to the ongoing geo-polymerization process, facilitated by immersing the samples in alkaline solutions for seven days. This extended exposure leads to the creation and maturation of more geo-polymeric products, thereby densifying the porous structures that are characteristic of the green samples.

Similar to the green samples, an anisotropic behaviour was noted concerning the postprocessed samples' compressive strength in relation to loading directions. Regardless of the fly ash content, the postprocessed samples consistently displayed higher compressive strength when measured in the X-direction compared to the Z-direction.

S100FA0 samples consistently shows the highest compressive strength, regardless of the testing direction and type of curing solution. With increase in the fly ash contents we can see reduction in the compressive strength of post-processed samples in both directions.

5. Conclusion

This study introduces a pioneering methodology for creating geopolymer-based materials tailored for use in commercially accessible 3D printers utilizing power technology and engineered for construction purposes. Through a comprehensive quantitative assessment, the study explored the impacts of various key powder parameters and the incorporation of fly ash on the printability and properties of those geopolymers which can be used for 3D printing. Following conclusions can be drawn from this research:

1. The geopolymer-based materials developed in this study exhibited favourable deposit ability and wettability, rendering them suitable replacements for commercially available printable materials in 3D printers which utilize powder, for construction purposes.
2. The fly ash quantity had minimal influence on the true, bulk, and in-process bed densities, as well as the powder bed porosity of the 3D printable geopolymer powders. Visual assessments indicated that all geo-polymer powders demonstrated adequate surface qualities conducive to the 3D Concrete Printing using powder (3D-CP) process.
3. The innovative postprocessing technique introduced in this study resulted in a significant augmentation of strength when contrasted with the initial levels. Specimens manufactured using 100% slag-based geopolymer powder exhibited the highest postprocessed compressive strength, reaching up to 29.6 MPa at the 7-day mark. A minimum of 50 wt% slag content was determined as necessary for the formulation of fly ash/slag-blended geopolymer powder suitable for the powder-based 3D-CP process. Postprocessed specimens produced with a composition of 50 wt% slag and 50 wt% fly ash powder achieved a 7-day compressive strength of up to 24.9 MPa.
4. Both the post-processed and green samples shows anisotropic characteristics in terms of compressive strength, contingent on the loading directions. In all instances, the strengths consistently displayed higher values when assessed in the X-direction compared to the Z-direction, regardless of the fly ash content.

The methodology devised in this study is inherently scalable, facilitating the fabrication of large-scale structural components through 3D printing utilizing powder technology.

REFERENCES

1. W. Gao, Y. Zhang, D. Ramanujan, K. Ramani, Y. Chen, C.B. Williams, et al., The status, challenges, and future of additive manufacturing in engineering, Comput. -Aided Des. 69 (2015) 65-89.
2. B. Berman, 3-D printing: the new industrial revolution, Business Horizons 55 (2012) 155-162.
3. I. Hager, A. Golonka, R. Putanowicz, 3D printing of buildings and building components as the future of sustainable construction? Procedia Eng. 151 (2016) 292-299.
4. S. Lim, R.A. Buswell, T.T. Le, S.A. Austin, A.G. Gibb, T. Thorpe, Developments in construction-scale additive manufacturing processes, Autom. Constr. 21 (2012) 262-268.
5. T. Wangler, E. Lloret, L. Reiter, N. Hack, F. Gramazio, M. Kohler, et al., Digital concrete: opportunities and challenges, RILEM Tech. Lett. 1 (2016) 67-75.
6. B. Khoshnevis, S. Bukkapatnam, H. Kwon, J. Saito, Experimental investigation of contour crafting using ceramics materials, Rapid Prototyping J. 7 (2001) 32-42.
7. B. Khoshnevis, D. Hwang, K.-T. Yao, Z. Yeh, Mega-scale fabrication by contour crafting, Int. J. Ind. Syst. Eng. 1 (2006) 301-320.
8. S. Lim, T. Le, J. Webster, R. Buswell, S. Austin, A. Gibb, et al., Fabricating construction components using layer manufacturing technology, 2009.
9. S. Lim, R.A. Buswell, T.T. Le, R. Wackrow, S.A. Austin, A.G. Gibb, et al., Development of a viable concrete printing process, 2011.
10. E.M. Sachs, J.S. Haggerty, M.J. Cima, P.A. Williams, Three-dimensional printing techniques, U.S. Patent No. 5,204,055. Washington, DC: U.S. Patent and Trademark Office., 1993.
11. G. Cesaretti, E. Dini, X. De Kestelier, V. Colla, L. Pambaguian, Building components for an outpost on the Lunar soil by means of a novel 3D printing technology, Acta Astronaut. 93 (2014) 430-450.
12. R. Rael, V. San Fratello, Developing concrete polymer building components for 3D printing, in: ACADIA. 31st Annual Conference of the Association for Computer Aided Design in ArchitectureBanff, 2011.
13. J. Davidovits, Geopolymers, J. Thermal Anal. Calorim. 37 (1991) 1633-1656.
14. P. Duxson, A. Fernández-Jiménez, J.L. Provis, G.C. Lukey, A. Palomo, J.S.J. Deventer, Geopolymer technology: the current state of the art, J. Mater. Sci. 42 (2006) 2917-2933.
15. B. Nematollahi, J. Sanjayan, F.U.A. Shaikh, Synthesis of heat and ambient cured one-part geopolymer mixes with different grades of sodium silicate, Ceram. Int. 41 (2015) 5696-5704.
16. M. Asadi-Eydivand, M. Solati-Hashjin, S.S. Shafiei, S. Mohammadi, M. Hafezi, N. A.A. Osman, Structure, properties, and in vitro behavior of heat-treated calcium sulfate scaffolds fabricated by 3D printing, PLoS One 11 (2016) e0151216.
17. A. Butscher, M. Bohner, C. Roth, A. Ernstberger, R. Heuberger, N. Doebelin, et al., Printability of calcium phosphate powders for three-dimensional printing of tissue engineering scaffolds, Acta Biomater., 8 (2012) 373-385.
18. Z. Zhou, F. Buchanan, C. Mitchell, N. Dunne, Printability of calcium phosphate: Calcium sulfate powders for the application of tissue engineered bone scaffolds using the 3D printing technique, Mater. Sci. Eng. 38 (2014) 1-10.
19. B. Utela, D. Storti, R. Anderson, M. Ganter, A review of process development steps for new material systems in three dimensional printing (3DP), J. Manuf. Process. 10 (2008) 96-104.
20. B.R. Utela, D. Storti, R.L. Anderson, M. Ganter, Development process for custom three-dimensional printing (3DP) material systems, J. Manuf. Sci. Eng., Trans. ASME 132 (2010) 0110081-0110089.
21. K.P. Hapgood, J.D. Litster, S.R. Biggs, T. Howes, Drop penetration into porous powder beds, J. Colloid Interface Sci. 253 (2002) 353-366. Development of Powder-Based 3D Concrete Printing Using Geopolymers 239
22. E. Nefzaoui, O. Skurtys, Impact of a liquid drop on a granular medium: inertia, viscosity and surface tension effects on the drop deformation, Exp. Thermal Fluid Sci. 41 (2012) 43-50.
23. Y. Shanjani, Y. Hu, R.M. Pilliar, E. Toyserkani, Mechanical characteristics of solidfreeform-fabricated porous calcium polyphosphate structures with oriented stacked layers, Acta Biomater. 7 (2011) 1788-1796.